Transcriptional Profiling of Xenogeneic Transplants: Examining Human Pluripotent Stem Cell-Derived Grafts in the Rodent Brain

Christopher R. Bye,[1,2,*] Vanessa Penna,[1,2] Isabelle R. de Luzy,[1] Carlos W. Gantner,[1] Cameron P.J. Hunt,[1] Lachlan H. Thompson,[1] and Clare L. Parish[1,*]

[1]The Florey Institute of Neuroscience and Mental Health, The University of Melbourne, Parkville, VIC, Australia
[2]Co-first author
*Correspondence: chris.bye@florey.edu.au (C.R.B.), clare.parish@florey.edu.au (C.L.P.)
https://doi.org/10.1016/j.stemcr.2019.10.001

SUMMARY

Human pluripotent stem cells are a valuable resource for transplantation, yet our ability to profile xenografts is largely limited to low-throughput immunohistochemical analysis by difficulties in readily isolating grafts for transcriptomic and/or proteomic profiling. Here, we present a simple methodology utilizing differences in the RNA sequence between species to discriminate xenograft from host gene expression (using qPCR or RNA sequencing [RNA-seq]). To demonstrate the approach, we assessed grafts of undifferentiated human stem cells and neural progenitors in the rodent brain. Xenograft-specific qPCR provided sensitive detection of proliferative cells, and identified germ layer markers and appropriate neural maturation genes across the graft types. Xenograft-specific RNA-seq enabled profiling of the complete transcriptome and an unbiased characterization of graft composition. Such xenograft-specific profiling will be crucial for pre-clinical characterization of grafts and batch-testing of therapeutic cell preparations to ensure safety and functional predictability prior to translation.

INTRODUCTION

Since the derivation of human pluripotent stem cell (hPSC) lines, there has been great hope and anticipation for the use of these cells and their derivatives in regenerative medicine. One of the most anticipated applications is their restricted fate specification to defined cellular populations for the purpose of transplantation, aimed at treating acute and chronic disorders. Some of the most advanced examples are hPSC-derived islet cells for the treatment of diabetes, retinal pigment epithelia for application in visual impairment conditions, and dopamine neurons for the replacement of those cells lost to Parkinson's disease (PD) (Trounson and McDonald, 2015).

Prior to clinical translation of hPSC-derived cells, it will be imperative that graft composition is well defined to ensure safety and functional predictability. The significance of understanding graft composition is perhaps most evidently demonstrated in hPSC-derived dopamine (DA) progenitor transplantation studies in PD models. Despite significant advancements in differentiation protocols resulting in high yields of correctly specified progenitors for grafting (Kirkeby et al., 2012; Kriks et al., 2011; Niclis et al., 2017b), following protracted graft analysis (>6 months) only a fraction of the transplant is composed of mature DA neurons (Doi et al., 2014; Kirkeby et al., 2012, 2017; Kriks et al., 2011; Niclis et al., 2017a; Samata et al., 2016). Such outcomes suggest that the small proportion of poorly specified cells present in the cultures subsequently expands following transplantation to dominate the graft. Histochemical assessment has been able to

confirm that these grafts are predominantly "neural" in origin and of an appropriate regional identity (Kriks et al., 2011; Samata et al., 2016); however, due to limited antibody availability to selectively assess the human cells, as well as not knowing what to specifically look for, the identity of much of these grafts remains unknown. This raises the concern of what impact these cells may have on graft function as well as on the host.

Transcriptionally profiling grafts has been hindered by the inability to selectively isolate the graft, which is interdispersed with the host tissue. When the graft can be clearly identified, (e.g., grafts of reporter stem cell lines), careful laser-capture microdissection can reduce the level of contaminating host cells. However, laser-capture-based approaches are labor intensive, require meticulous tissue processing to maintain RNA quality, and are associated with low RNA yields. An alternative approach is isolating the grafted cells by tissue dissociation and applying fluorescent or magnetic cell-sorting strategies. This approach relies on the dissociation of post-mitotic cells and can result in poor survival. Single-cell genomic profiling of cells within the graft has also increasingly been employed to assess molecular and cellular diversity within defined populations (Etzrodt et al., 2014; La Manno et al., 2016; Tang et al., 2010). While providing an accurate assessment of the cell identity within the graft, such approaches are also onerous and sample just a fraction of the graft.

Circumventing these challenges, we develop here a method that employs a selective detection process to discriminate graft transcripts within a mixed graft-host tissue pool. This simple approach relies on identifying RNA

sequence differences between the host and graft species to design species-specific primers for the purpose of real-time qPCR, and similarly recognizing species-specific reads for RNA sequencing (RNA-seq). The utility and rigor of these techniques are demonstrated by comparing different transplant populations of human cells in the rodent brain.

RESULTS

Design and Validation of Xenograft-Specific Primers for Real-Time qPCR

To identify xenograft-specific sequences using qPCR, we designed primers targeting regions of dissimilarity between the two species (Figure 1A). Specifically, primers targeted an RNA sequence containing a minimum of 5-bp mismatches between xenograft and host, or two mismatches within the 5 bp at the 3′ end of the primer (e.g., Ki67 and LMX1A forward primers) (Figure 1B). To confirm the specificity of the primers for xenograft transcript, we tested primers with *in vitro* pools of mouse or human cells known to express the target genes. A total of 30 primers were designed and tested (Figure 1B). Primer specificity for xenograft transcripts (over mouse) ranged from 500 to 1.0×10^7 times greater, with a median specify of 174,000 (Figure 1C). Using an arbitrary cutoff of 1,000 times (1,000×) greater specificity for the human pool compared with mouse, primers for 97% of genes (29/30) were deemed as specific.

With success at designing species-specific primers, as validated *in vitro*, next the feasibility of this approach *in vivo* was determined, targeted at confirming the ability to discriminate between xenograft and host transcripts. To achieve this, we analyzed transplants of human stem cells in the striatum of immune-compromised athymic mice using qPCR. The specificity of the primers for xenograft RNA were confirmed *in vivo* by measuring the ability to detect the expression of four constitutively expressed genes in grafted tissue compared with ungrafted tissue (i.e., mouse striatal tissue containing no xenograft) (Figure 1D). The four primers tested specifically detected xenograft transcripts *in vivo*, with expression in the grafted host greater than the host-only tissue for PSMB4 (10,349×), MTHFD (769×), CHAMP2A (2,775×), and HPRT1 (1,726×).

To access the capacity of species-specific primers to provide a readout of graft size, we implanted a known number of neural progenitors (10,000, 30,000, 100,000, or 300,000 cells) into the rodent brain and assessed the expression levels of housekeeping genes after 2 weeks. A xenograft-specific primer for a housekeeping gene was used to assess graft size, while a host-specific primer enabled assessment of the amount of host tissue present within the isolated tissue. Expressed as a proportion of total RNA, xenograft RNA constituted 0.8% ± 0.60% (10,000 cells), 6.5% ± 2.48% (30,000 cells), 12.8% ± 1.78% (100,000 cells), or 18.1% ± 3.31% (300,000 cells) of the RNA population (Figure 1E). The estimate of xenograft RNA showed a tight and significant correlation with the number of cells transplanted ($r^2 = 0.78$), demonstrating the utility of the method to rapidly estimate graft size.

Characterization of Xenografts Using Species-Specific Real-Time qPCR

To demonstrate and validate the utility of species-specific transcriptional profiling of xenografts, we compared RNA from three distinct xenografts: (1) grafts derived from undifferentiated PSCs, anticipated to contain proliferative populations and cells from all three germ layers after 1 month *in situ* (subsequently referred to as the "undifferentiated" grafts); (2) transplants of ventral midbrain (VM) neural progenitors, analyzed 1 month after implantation and anticipated to show characteristic signatures of immature neuronal progenitor neurons (subsequently referred to as "immature neuronal" grafts); and (3) grafts of VM neural progenitors, allowed to mature for 5 months *in situ* into neuronal populations inclusive of dopamine neurons (denoted "mature neuronal" grafts). In parallel, tissue was collected from separate animals for immunohistochemistry to provide verification of the gene-expression results.

Using an antibody specific for human cells (human nuclear antigen [HNA]) that enabled delineation of the graft, size and cell number were determined. Grafts of undifferentiated cells were large and expansive (7.0 ± 3.5 mm³ containing $2.03 \times 10^6 \pm 0.43 \times 10^6$ cells), while immature neuronal grafts were small (0.43 ± 0.07 mm³ with $0.49 \times 10^5 \pm 0.11 \times 10^5$ cells), and of moderate size following ongoing maturation (mature neuronal grafts: 2.4 ± 0.25 mm³ containing $1.51 \times 10^5 \pm 0.31 \times 10^5$ cells) (Figures 2A–2D). Transcriptional estimation of graft size, by xenograft-specific qPCR, measured the proportion of xenograft RNA at 33.0% ± 8.9% in the undifferentiated grafts, 1.8% ± 0.4% in the immature neuronal grafts, and 9.2% ± 0.9% in the mature neuronal grafts (Figure 2E), reflective of graft sizes determined histologically.

Necessary for the safe clinical translation of cell transplantation is the removal of proliferative cells prior to implantation, or their reduction to low levels shortly thereafter. Hence, in an effort to characterize graft composition, the expression of the proliferative gene *Ki67* was assessed. A large population of Ki67⁺/HNA⁺ dividing cells were identified in the undifferentiated grafts (9.5% ± 1.0%) that was significantly reduced in immature neuronal grafts (0.74% ± 0.16%) and reduced further in the mature neuronal grafts (0.28% ± 0.06%) (Figures 2A–2C and 2F). Xenograft-specific gene expression (expressed relative to
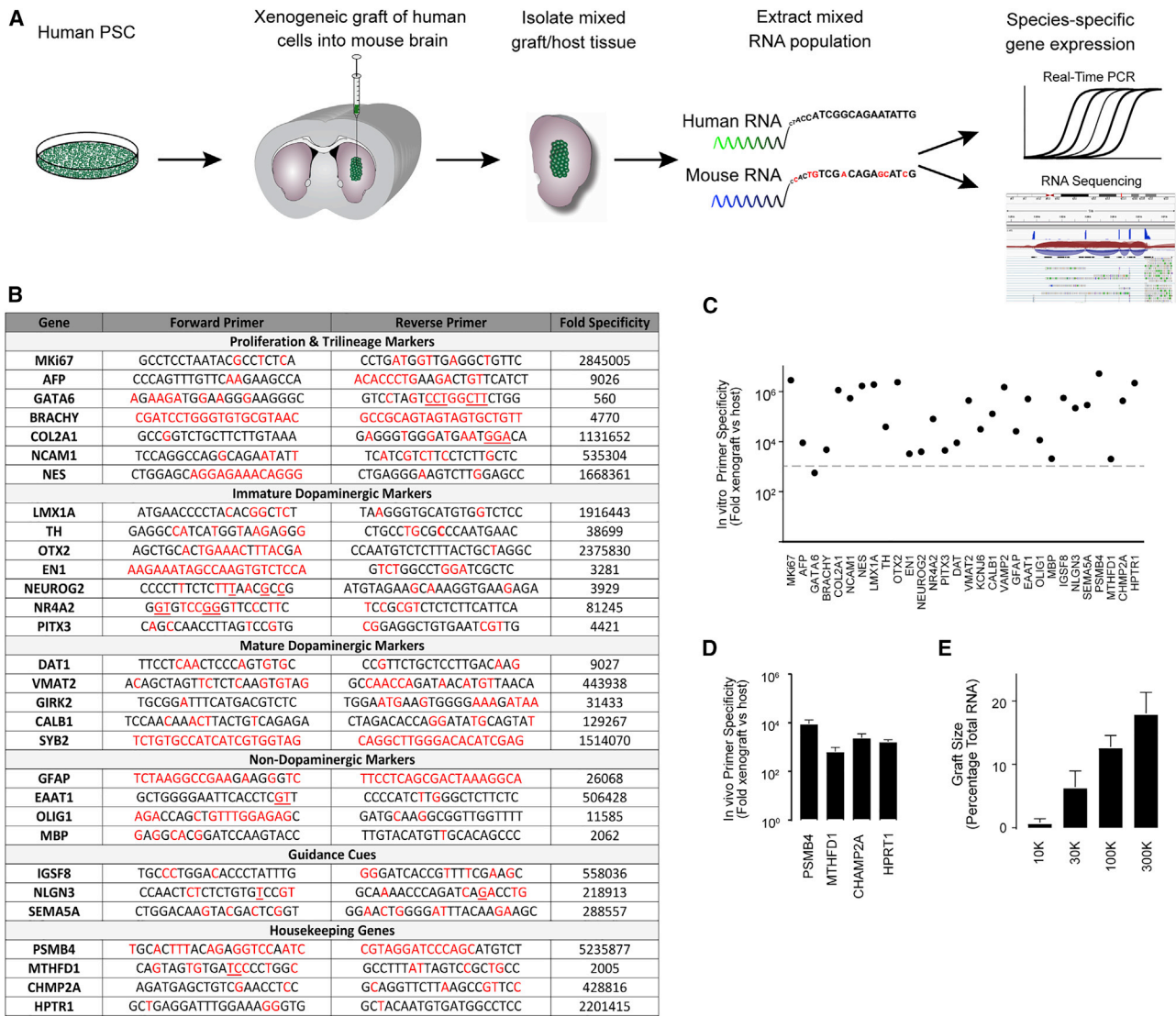
Figure 1. Design and Validation of Xenograft-Specific Primers for Real-Time qPCR

(A) Schematic of the experimental paradigm. hPSC-derived cells were transplanted into the rodent brain. Tissue containing both transplanted cells and host tissue was dissected, and the RNA isolated to produce a mixed-species RNA pool. Xenograft gene expression was discriminated from the host using species-specific primers for qPCR, or by RNA-seq to profile the entire genome.

(B) Table of human xenograft-specific primers designed for the present study. Nucleotide bases shown in red correspond to mismatches between the human and mouse RNA sequence, and underlined bases represent the presence of insertions or deletions.

(C) Graph of the specificity of xenograft-specific primers for human transcript relative to rodent host transcript *in vitro* showing an average specificity of 5,000 times that of the host (also represented numerically as "fold specificity" in B). An arbitrary cutoff of 1,000-fold (gray line) represents an ideal specificity threshold, with 96% of primers designed in this study exceeding this threshold.

(D) *In vivo* specificity of xenograft-specific primers for four constitutively expressed transcripts, showing an average specificity of ~4,000 times greater in the transplanted compared with untransplanted host.

(E) Estimation of xenograft size using a xenograft-specific primer, PSMB4, showed a significant correlation ($r^2 = 0.78$) with actual number of cells implanted into the host.

Data in (D) and (E) represent mean ± SEM, n = 4 grafts/group.

the undifferentiated grafts) showed that Ki67 expression in the immature grafts was reduced to 0.11 ± 0.02-fold, and to 0.05 ± 0.01-fold in mature grafts (Figure 2G), corresponding closely to the cell counts, and highlighting the capacity for xenograft-specific qPCR to detect rare cell populations.
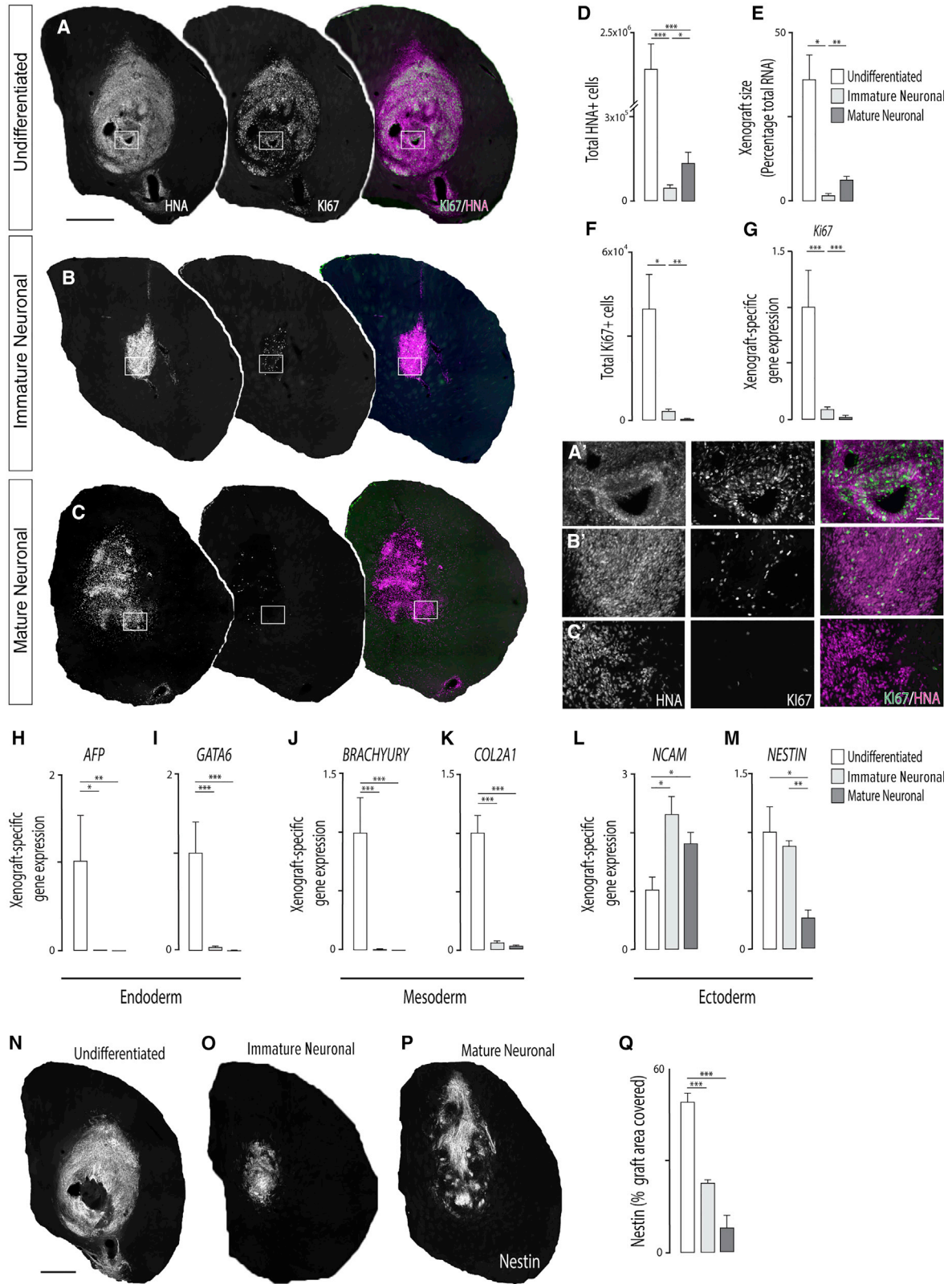
(legend on next page)

The capacity of the technique to detect different cellular populations within a graft was demonstrated using primers targeted against genes restricted to defined germ layers (endoderm, mesoderm, and ectoderm) (Tsankov et al., 2015; D'Antonio et al., 2017). Unsurprisingly, endoderm (AFP and GATA6) and mesoderm (Brachyury and Collagen2A type 1, COL2A1) genes were lowly expressed in the immature and mature neuronal grafts (Figures 2H–2K). In contrast, expression of the ectoderm marker neural cell adhesion marker (NCAM) was elevated in the immature and mature neuronal grafts (2.25 ± 0.39 and 1.58 ± 0.38, respectively) (Figure 2L). The neuroectodermal stem cell marker, Nestin, expressed in the immature neuronal grafts, was reduced in the mature graft, reflective of downregulation of the gene during neuronal maturation as observed in development (Wiese et al., 2004) (Figure 2M) and confirmed by Nestin immunohistochemistry (Figures 2N–2Q). Greater differences in neuroectodermal gene expression between the undifferentiated and neuronal fate-restricted grafts (immature neuronal and mature neuronal) were not observed, largely due to the preferential default neural fate acquisition of PSCs (Munoz-Sanjuan and Brivanlou, 2002).

Next, the sensitivity of the approach to detect more subtle changes present between immature neuronal and mature neuronal grafts was assessed. Immunohistochemistry against GFP (to identify the LMX1A-GFP$^+$ cells) and TH (tyrosine hydroxylase) identified immature VM neural progenitors and mature dopaminergic neurons, respectively (Figures 3A–3C). Counts revealed that $21\% \pm 4\%$ of cells in the undifferentiated grafts expressed GFP, a proportion that was enriched in the immature neuronal grafts ($82\% \pm 1\%$) and maintained in the mature neuronal grafts ($76\% \pm 4\%$) (Figure 3D). Xenograft-specific gene expression showed that LMX1A was increased 32.7 ± 1.7-fold in the immature neuronal grafts, and reduced 17.2 ± 2.3-fold in the mature neuronal grafts (Figure 3E), commensurate with the cell counts and in accordance with the previously

described downregulation of the gene in maturing midbrain dopamine neurons during development. Counts of the mature dopaminergic marker TH identified $0.3\% \pm 0.04\%$ cells in the undifferentiated grafts (TH$^+$/HNA$^+$), significantly increased in the immature neuronal grafts ($4.4\% \pm 1.5\%$), and further increased in the mature neuronal grafts ($7.2\% \pm 0.9\%$) (Figure 3F). Xenograft-specific gene-expression analysis supported the increase in TH with expression 8- and 12-fold greater in the immature and mature neuronal grafts, respectively, compared with those of undifferentiated cells (Figure 3G).

To demonstrate the utility of the approach to rapidly and comprehensively profile graft composition, we assessed nine additional genes anticipated to be expressed predominantly in neural specified grafts. Four genes expressed within VM neural progenitors included the midbrain-hindbrain restrictive gene Engrailed-1 (EN1), forebrain-midbrain gene OTX2, dopaminergic precursor Nurr1 (NR4A2), and pro-survival gene PITX3 (Figures 3H–3K). As expected, in comparison with undifferentiated grafts, upregulation of OTX2 (3-fold) and NR4A2 (16-fold) were observed in the immature neuronal grafts (rich in dopaminergic progenitors) but not the more mature (dopaminergic neuronal) grafts, reflective of the transient expression of these genes in embryonic development (Niclis et al., 2017b). PITX3 was upregulated in both the immature and mature neuronal grafts compared with the undifferentiated grafts. Surprisingly, EN1 was downregulated in the neuronal grafts, a result that likely reflects its many roles in early development inclusive of embryonic segmentation and limb formation. The five mature neuronal genes examined included G-protein-regulated inward-rectifier potassium channel 2 (GIRK2/KCNJ6) and Calbindin-1 (CALB1), markers of mature midbrain dopamine neuron subpopulations; dopamine transporter (DAT/SLC6A3) and vesicular monoamine transporter 2 (VMAT2/SLC18A2), both responsible for dopamine recycling; and vesicle-associated membrane protein Synaptobrevin

Figure 2. *In Vivo* Validation of a Xenograft Profile Using Species-Specific qPCR

(A–C) Representative micrograph depicting a graft of undifferentiated hPSCs 1 month after implantation (A), an immature neuronal graft at 1 month (B), and a mature neuronal graft at 5 months (C). Human nuclear antigen (HNA) labeled all human donor cells within the host, while Ki67 labeled proliferative cells.

(D and E) Quantification of HNA$^+$ cells within the grafts (D) closely mirrored the proportion of human-specific transcript (as a percentage of total transcript) (E).

(F and G) Quantification of Ki67$^+$ proliferative cells, significantly elevated in grafts of undifferentiated hPSC (F), reflected RNA transcript levels of the gene (G).

(H–M) Trilineage specification of cells within grafts of undifferentiated hPSCs was demonstrated by high transcript expression of endoderm (AFP, GATA6), mesoderm (BRACHYURY, COL2A1), and ectoderm (NCAM, NESTIN) genes. Appropriately, neural progenitor grafts (immature and mature neuronal grafts) contained only neuroectodermal gene expression.

(N–P) Representative images of NESTIN-immunoreactive cells.

(Q) Comparative levels of Nestin transcript were validated by the proportion of the graft showing NESTIN immunoreactivity.

Data in (D–G), (H–M), and (Q) represent mean $\pm$ SEM, one-way ANOVA, n = 5 grafts/group. Scale bars, 500 μm (A–C, N–P) and 100 μm (A'–C').

Figure 3. Validation of Midbrain Dopaminergic Identity of Xenografts Using qPCR

(A–C) Representative images from an undifferentiated hPSC (A), immature neuronal (B), and mature neuronal (C) graft depicting immunohistochemical expression of the early VM progenitor protein LMX1A (using an LMX1A-GFP reporter cell line) and mature dopamine neuron protein tyrosine hydroxylase (TH).

(D and E) Neural specification of the cells prior to transplantation (to a VM dopaminergic identity) (D) resulted in a significant increase in LMX1A-labeled cells that could be validated by species-specific LMX1A expression (E).

(F and G) Similarly, TH cell counts significantly increased within ongoing maturation of the neuronal grafts (F) compared with undifferentiated cell grafts (G), results that were validated by TH qPCR.

(legend continued on next page)

2 (SYNB/VAMP2), a mature presynaptic protein (Figures 3L–3P). Both GIRK2 and CALB1 were significantly increased in the immature and mature neuronal grafts. Not surprisingly, synaptic protein and transmitter associated genes DAT (49-fold), VMAT, and SYB2 showed significantly elevated expression in mature neuronal grafts compared with undifferentiated and immature neuronal grafts. The increased synaptic integration of the mature neuronal grafts was supported by increased histochemical labeling for human synaptophysin in mature (Figure 3R) compared with immature neuronal grafts (Figure 3Q).

Unbiased Characterization of Xenograft Composition and Identification of Transcriptional Changes Using RNA-Seq

Expanding on our species-specific transcript profiling approach, we sought to demonstrate the capacity for high throughput gene expression profiling using RNA-seq. Unlike qPCR, RNA-seq enables unbiased characterization of graft composition, confirming both known/anticipated gene expression and the presence of previously unidentifiable cell populations. RNA-seq can also provide new insight into gene expression, including recognition of mechanistic pathways contributing to graft function. Mixed-species cDNA libraries were prepared from the three graft types and subjected to paired-end, 75-bp sequencing to a target depth of approximately 20 million human reads (using the estimation of percentage xenograft RNA described in Figure 2E). A rapid and computationally efficient analysis pipeline was then established and implemented on the freely available Galaxy platform to make it accessible without specialist bioinformatics infrastructure or expertise. Reads were first mapped against the human genome, with only concordant (successfully aligned) reads subsequently mapped to the mouse genome. To minimize the risk of incorrectly specified reads, we adopted a high-stringency approach whereby all human reads found to also map to the mouse genome were discarded. The retained reads were designated as unique to the human genome, and therefore originated from the xenograft. An average of 94.4% ± 1.5% of reads were identified as unique to the human genome under these criteria across the three graft groups (Figure 4A). An average of 5.6% ± 1.5% of reads aligned to both human and mouse genome and were therefore discarded from analysis. These discarded reads mapped

to 327 genes (defined as having an average of >10 reads) and showed no enrichment for any gene ontology category or pathway. Visual analysis of the ten most highly expressed genes from this list (Figures S2A–S2H) showed that the reads did not provide broad coverage across genes, aligning only to isolated fragments in both exonic and intergenic regions. The reads did not map preferentially to highly conserved regions or repeat elements, and displayed profiles consistent with originating from mouse RNA (significant mismatches to human genome, not overlapping with human-specific reads).

Taking advantage of the variation in graft size across the experimental groups, an estimate of the percentage of xenograft RNA required in the host tissue to provide a sufficient level of unique reads for analysis was assessed. Samples in which human RNA constituted just 2.5% of the total RNA (human RNA + mouse RNA) provided 86% reads unique to the human transcript using our high-stringency approach. This specificity increased exponentially such that with 6.7% human RNA, greater than 95% of the reads was classified as uniquely human, while grafts containing 35% human RNA yielded 99% unique reads (Figure 4B). Overall these results demonstrate that the analysis pipeline provided an efficient yield of species-specific reads from within a graft-host pool of tissue/RNA, including when the graft size was limited.

To determine whether the identified xenograft-specific reads were consistent with xenograft gene expression, we assembled transcripts for analysis. Examination of the global gene-expression profile by principal component analysis showed that the grafts clustered tightly as three distinct populations corresponding to the three grafted cell types (Figure 4C). A dissimilarity matrix and unsupervised clustering also showed the highest similarity between the replicates of each group, with immature neuronal and mature neuronal grafts the most closely related graft types (Figure 4D). Combined, these findings show that at a global expression level the xenograft-specific RNA-seq provided a highly specific expression profile consistent with the expected graft relationships.

To demonstrate the ability to use RNA-seq data to investigate known and unknown genes, we conducted xenograft-specific differential expression analysis (Figure 4E). A total of 11,010 differentially expressed genes were identified between the undifferentiated and

---

(H–P) Graft expression of early VM neural progenitor transgenes as revealed by species-specific qPCR primers for EN1 (H), OTX2 (I), NURR1 (J), PITX3 (K), as well as mature dopaminergic neuronal genes GIRK2 (L), CALB (M), DAT (N), VMAT (O), and SYNB (P).

(Q and R) Immunohistochemical labeling against TH (green) and human synaptophysin (hSYP, magenta) in immature (Q) and mature (R) neuronal grafts.

Data in (D–G) and (H–P) represent mean ± SEM, one-way ANOVA, n = 5 grafts/group. Scale bars, 500 μm (A–C), 200 μm (A and C′), and 50 μm (A″, C″, C‴, Q, and R).
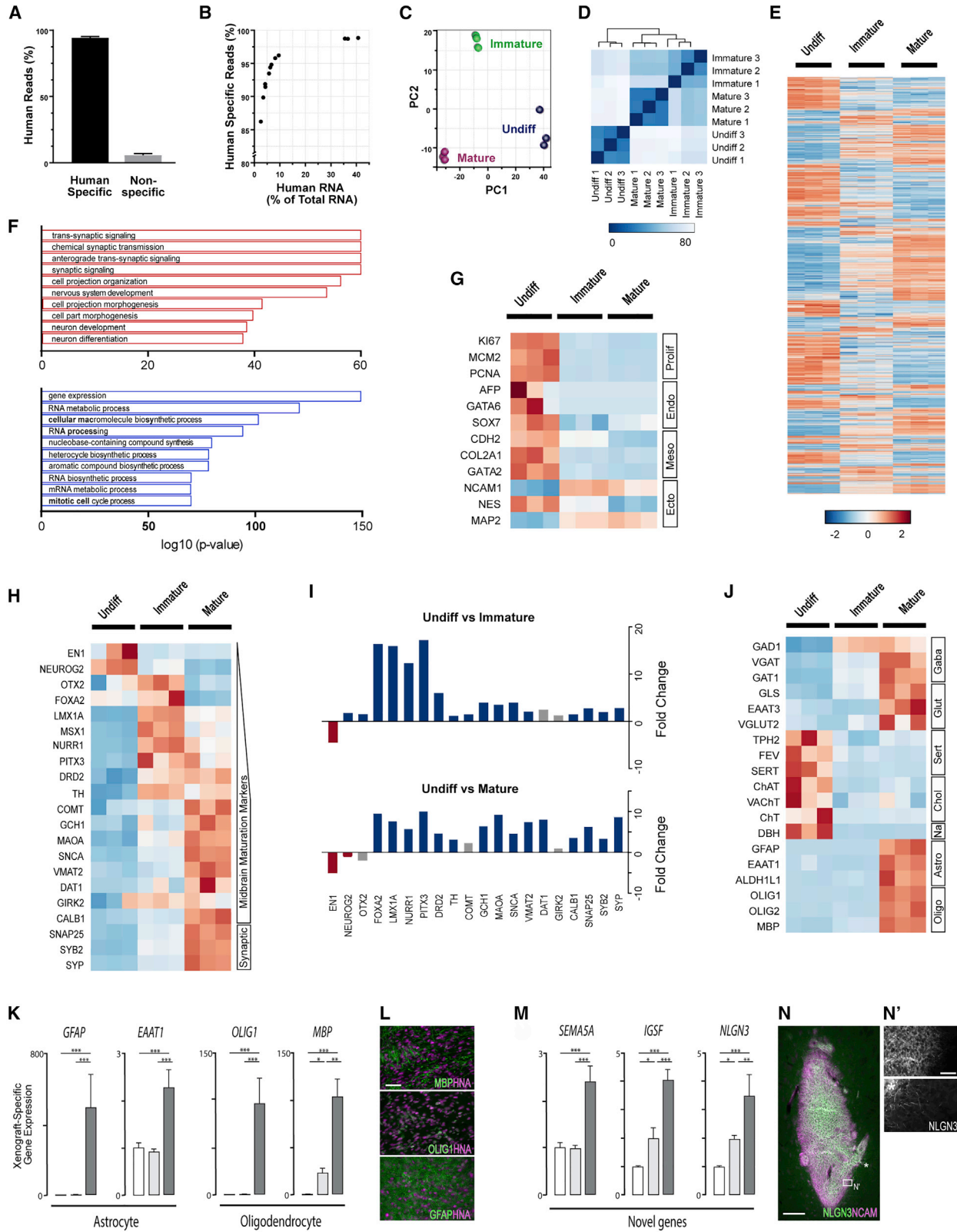
(legend on next page)

immature neuronal grafts (Table S1) and 12,449 genes between the undifferentiated and mature neuronal grafts (Table S2). Enriched gene ontology categories between undifferentiated and immature neuronal grafts identified upregulation of genes associated with synaptic signaling, axonal plasticity, and neural development, while RNA expression/processing and regulation of cell-cycle genes were downregulated (Figure 4F). Analysis of genes at this comparison identified 233 transcription factors potentially involved in the development of mature dopaminergic populations (Table S3), and 751 genes coding for axon guidance cues and receptors (Table S4), including several associated with the classical axon guidance superfamilies (Figure S3A). Many of the identified guidance cues have previously been implicated in dopamine axonal plasticity in rodents, but not yet in humans. These results provide an expansive list of targets for the potential modulation of cell populations or axon growth and plasticity in the maturation and integration of neuronal grafts.

The utility of the RNA-seq data to provide an unbiased characterization of the xenograft composition was first confirmed by assessment of known genes. Reflective of qPCR observations, Ki67 was highly expressed in the undifferentiated grafts (Figure 2G). Two additional pro-proliferation genes, DNA replication licensing factor MCM2 and proliferative cell nuclear antigen, were similarly upregulated (Figure 4G). Expression of three markers of an endodermal, mesodermal, and ectodermal lineage were all shown to be highly expressed in the undifferentiated

cell group. In accordance with qPCR findings, endodermal and mesodermal genes were downregulated in the immature and mature neuronal grafts, while ectodermal markers remained expressed or were downregulated with ongoing graft maturation, reflective of neural development. Further validating the approach, numerous vascular-associated genes, such as essential hematopoietic transcription factor TAL1 and vasculogenesis gene FLT1, were upregulated in the undifferentiated PSC grafts (i.e., teratomas) but not neural progenitor grafts, and could be validated by qPCR (Figure S4).

Genes of known association with dopamine development and function showed increased expression in immature and mature neuronal grafts compared with the undifferentiated. Expression levels were represented as a heatmap (Figure 4H) and graphed as fold change for each of the comparisons between the graft types (Figure 4I). Markers of dopamine progenitors NEUROG2, FOXA2, OTX2, and LMX1A were most highly expressed in the immature neuronal grafts. NR4A2, PITX3, TH, and DRD2 were maintained at high levels in the both immature and mature neuronal grafts, while the mature genes GCH1, MAOA, SNCA (α-synuclein), VMAT2/SLC18A2, and DAT1/SLC6A3 were expressed most highly in the mature neuronal grafts. Confirming graft maturation, synaptic markers SNAP25 (Synaptosome Associated Protein 25), Synaptobrevin2 (SYNB/VAMP2), and SYP (Synaptophysin) were all significantly upregulated in the immature neuronal grafts, with even greater fold changes in the mature neuronal grafts (Figure 4I).

Figure 4. Unbiased Characterization of Xenograft Composition and Identification of Transcriptional Changes Using RNA-Seq

(A) Graph showing that 94.4% of the RNA-seq reads were uniquely mapped to the human genome (xenograft-specific) compared with 5.6% mapping to both human and host (ambiguous origin).

(B) Graph of the percentage of xenograft-specific reads compared with the size of the xenograft, showing that xenografts contributing ≥2.5% of the total RNA provide greater than 86% uniquely identified xenograft reads.

(C) Principal component analysis comparing the global gene-expression profile of each xenograft revealed the samples clustered into three distinct groups corresponding to the three graft types.

(D) A dissimilarity matrix of the global RNA profile correlation and unsupervised clustering showed the highest similarity between the replicates of each group.

(E) Heatmap of xenograft-specific gene expression.

(F) Graph of enriched gene ontology categories between undifferentiated and immature neuronal grafts.

(G) Heatmap of markers of germ layer lineages across the different graft types.

(H and I) Heatmap (H) and fold change (I) in gene expression for early and late VM dopaminergic neuron markers across the three graft types.

(J) Heatmap of non-dopaminergic neural cell type markers across the three graft types.

(K) Real-time qPCR verification of the expression of astrocyte (GFAP, EAAT1) and oligodendrocyte (OLIG1, MBP) genes.

(L and M) Representative immunohistochemistry (L) confirmed the presence of astrocytes and oligodendrocytes in the mature grafts. RNA-seq (M) identified a number of previously unidentified genes expressed in the mature neuronal grafts that could be verified by qPCR (SEMA5A, IGSF8, NLGN3).

(N) Immunohistochemical staining against NLGN3 (green) and human-specific NCAM confirmed the presence of this plasticity-associated gene within the mature neuronal grafts.

Data represent mean ± SEM, one-way ANOVA. (A–J) n = 3 grafts/group, (K and M) n = 5 grafts/group. Scale bars, 50 μm (L and N′) and 250 μm (N).

With less than 5% of VM neural progenitor grafts consisting of dopamine neurons, and yet little knowledge of the identity of the remaining >95% of cells, the dataset was screened for markers of other neural (non-dopaminergic) cell populations in the three grafted cell groups (Figure 4J). GABAergic (GAD1, VGAT/SLC32A1, GAT-1/SLC6A1) and glutamatergic (GLS, EAAT2/SLC1A2, VGlut2/SLC17A6) related genes were found to be expressed in the mature neuronal grafts, suggestive of the presence of these neuronal populations, while low expression of serotoninergic (TPH2, FEV, SERT/SLC6A4), cholinergic (ChAT, VAChT/SLC18A3, Ch/TSLC5A7), and noradrenergic (DBH) relative to undifferentiated grafts inferred that few of these neuronal populations were present within midbrain-differentiated grafts. Strikingly, non-neuronal cell types showed unexpectedly high expression within mature grafts, including astrocyte-associated genes GFAP, GLAST/SCL1A3, and ALDH1L1 as well as oligodendrocyte genes OLIG1, OLIG2, and MBP (Figure 4J). Xenograft-specific qPCR profiling and immunohistochemistry for the astrocyte markers GFAP and EAAT1/SLC1A3 as well as oligodendrocyte markers OLIG1 and MBP confirmed the presence of these cell populations in the mature grafts (Figures 4K and 4L). Retrospective assessment of matured VM progenitor grafts from four previous grafting studies performed in the laboratory validated and confirmed the significant proportions of these glial populations within grafts (data not shown). The identification of non-target cell types in the mature grafts demonstrates the utility of using xenograft-specific profiling to screen a broad range of phenotypic markers and cell populations.

Finally, the dataset was utilized to detect unique candidate genes that may participate in the maturation and plasticity of human PSC-derived VM progenitor grafts. We identified and examined three genes that show significantly elevated expression within the mature neuronal graft: SEMA5a (Semaphorin 5A), IGSF8 (Immunoglobulin superfamily member 8), and NGLN3 (Neuroligin 3). Each of these genes were confirmed by qPCR (Figure 4M) and NGLN3 further validated by immunohistochemistry, showing punctate expression throughout the graft and evident along graft-derived axonal fibers (Figures 4N and 4N′). A lack of reliable commercially available antibodies against Semaphorin A5 and IGSF8 prevented confirmation of expression at the protein level. These findings provide the first efforts and evidence for identifying the true composition of VM neural progenitor grafts and highlight the utility for this transcriptional profiling methodology in understanding graft composition. In the present context, the identification of new genes involved in graft maturation may present candidate proteins for manipulation in the future, targeted at promoting graft plasticity, integration, and function.

DISCUSSION

Here, we describe an approach to transcriptionally profile xenografts by discriminating the graft species RNA from host. The technique is designed to allow standardization and characterization of graft composition. The method is simple to implement, requires minimal experience, and is highly reproducible. The rapid design of primers and large quantity of RNA generated allows a greatly enhanced number of genes to be measured in a relatively short time frame, enabling a more thorough characterization of grafts inclusive of proteins/genes that are currently difficult to discriminate. When combined with RNA-seq, the technique provides an unbiased means to screen graft composition, investigate key questions pertaining to their function, and provide insight into strategies to enhance grafting outcomes.

Within this study we demonstrated the utility of this technique by analyzing three distinct human grafts within the rodent brain: grafts derived from undifferentiated hPSCs, grafts of immature neural progenitors, and grafts of neural progenitors left to mature *in situ* over several months. Xenograft-specific qPCR and RNA-seq were both demonstrated to accurately and efficiency discriminate xenograft gene expression from host. In addition, to cross-validate these qPCR and RNA-seq outcomes, we confirmed findings by immunohistochemistry, where antibodies were available, with quantification across the three methodologies generating highly correlated results.

Validated both *in vitro* and *in vivo*, the specificity of xenograft-specific (human) qPCR primers designed for the 30 genes examined in the present study showed 1,000- to >1,000,000-fold increased expression over the mouse host. As such, the technique allowed the presence of a xenograft to be confirmed and provided an estimate of the graft size. The proportion of xenograft RNA in individual pools of both graft and host tissue correlated with pre-determined cell numbers, while cell counts in experimental groups quantified in parallel using immunohistochemistry also closely matched these estimates, as did the proportion of xenograft RNA estimated by RNA-seq. The technique was also able to accurately detect both large- and small-scale changes in graft cell populations, such as the expression of germ layer lineage-specific markers in undifferentiated cell grafts, compared with the more subtle changes between immature and mature neuronal grafts.

A key advantage of this transcriptional profiling approach is the ease of tissue and RNA isolation, allowing standardization across laboratories and by separate operators. Here, grafts were placed into the striatum as it provided an easily identifiable structure for gross tissue dissection, yet gratfs could be transplanted in any location.

Following gross tissue dissection, RNA was readily isolated using a standard column-based protocol. The large amount of tissue ensured that the RNA extraction was robust against the effects of RNA loss or degradation and allowed the RNA quality and quantity to be analyzed using the commonly available nanodrop spectrophotometer. The mixed-species RNA population could then be directly interrogated with PCR or RNA-seq, making the process easily achievable for most laboratories without necessary expertise in microdissection, single-cell sorting, or RNA handling. To make the RNA-seq analysis methods employed here accessible without specialist bioinformatics experience or infrastructure, we implemented the analysis pipeline in the freely available Galaxy web platform (www.usegalaxy.org/), which provides point-and-click access to all the required bioinformatics tools (Afgan et al., 2018).

Analysis of graft composition is often hindered by the availability of reliable antibodies, or the presence of a protein of interest in both the graft and host tissue, thereby preventing the ability to discriminate the graft. This latter challenge is especially relevant when cells migrate and intersperse within host tissues or, in the context of neural transplants, when axons innervating regions distal to the site of implantation cannot be accurately separated. Xenograft-specific qPCR can readily detect any gene of interest in a graft, irrespective of the expression in the host or localization of the cell within surrounding tissues. As evidence, here we successfully designed primers against NURR1/NR4A2, EN1, and PITX3, examples where antibodies are unavailable or unreliable. Primers were also designed against genes expressed in both the graft and host tissue for which human-specific antibodies are not available, including broadly expressed neural (Nestin and GFAP), dopamine-specific (TH, DAT1/SLC6A3 and VMAT2/SLC18A2), and synaptic genes (SYB2/VAMP2). Added to this was the ability to detect rare events within transplants, such as proliferative Ki67 cells. Importantly, validity of the species-specific qPCR technique was demonstrated by similarities in gene-expression levels and cell counts within the grafts.

The inability to easily apply high-throughput gene or protein analysis to xenografts has been a major impediment to understanding graft integration and to identifying targets to enhance survival, maturation, and plasticity that may affect overall graft function. Xenograft-specific RNA-seq provides an easily accessible tool for the interrogation of the entire transcriptome of the transplant, allowing the investigation of previously unknown genes and pathways active in the graft. Importantly, the RNA-seq data also contain host-specific reads, thereby providing the means to examine interactions between the host tissue and the xenograft. Here, we have described the ability of xenograft-specific profiling to characterize graft composition. The ability to measure all the expressed genes in the graft

allows an unbiased assessment and the ability to rapidly screen a range of cell phenotypes. No prior assumptions are required (as with antibody selection or qPCR primer design). The capture of all genes allows an expanded examination of markers, providing a thorough analysis of the target cell populations. The advantage of an unbiased and thorough coverage of phenotypic markers was exemplified here by the surprising expression of astrocyte and oligodendrocyte transcripts within grafts derived from fluorescence-activated cell sorting (FACS)-sorted VM neural progenitors. The presence of these cell types predominantly in mature grafts highlights the importance of long-term transplantation to accurately access the efficiency of differentiation protocols. The presence of small pools of poorly specified cells can expand to become a significant component of the graft at therapeutically relevant time frames, yet are not easily detected *in vitro*. These cell types are difficult to detect using conventional approaches, as host astrocyte and oligodendrocyte cells can migrate to infiltrate the graft and can only be directly detected using transgenic reporters. As the use of transgenic reporters is not feasible in a clinical setting, xenograft-specific profiling may present the only approach for pre-clinical testing of cell-differentiation protocols and cell batch verification prior to transplantation in patients. This is especially relevant in light of the two recently commenced clinical trials (Cyranoski, 2018; Barker et al., 2017) that adopt similar differentiation protocols to the one used here for the generation of midbrain dopamine neurons in the treatment of PD.

Finally, we demonstrated the utility of the species-specific RNA-seq approach in identifying previously unidentified genes within grafts. Here, we identified the expression of Nlgn3, Sema5A, and IGSF8 within mature neuronal grafts (compared with immature). These proteins have previously been implicated in axonal and synaptic plasticity (Bariselli et al., 2018; Kantor et al., 2004) or shown to be expressed on dopaminergic progenitors (Bye et al., 2015), but their roles in dopaminergic graft maturation remains to be explored. With previous work showing that hPSC-derived dopamine neurons show inferior plasticity to grafts derived from fetal tissue, identification of such genes may present new targets for modulating axonal growth and graft integration.

While we highlight the many benefits of whole tissue xenograft-specific transcriptomics, we also acknowledge the limitations. Unlike in single-cell sequencing, the transcript levels of individual cells are not captured individually. This restricts the classification of complex cell populations in the graft, with the xenograft-specific expression profile reflecting expression over the entire graft and unable to identify how many cells express a given gene or the level of expression within each cell. The approaches described here are thus highly complementary. One also recognizes that while RNA-seq profiling of the grafts is highly sensitive

and informative, it can also be expensive, especially when attempting to detect low numbers of grafted cells.

In summary, we describe an alternative approach to profiling xenografts. While demonstrated in the context of PSC-derived dopamine grafts for cell therapy in PD, this technique holds promise for profiling all xenografts, both within and outside the brain.

EXPERIMENTAL PROCEDURES

Cell Culture, Differentiation, and Sorting

Mouse RNA, containing mixed cell populations, inclusive of naive PSCs through to maturing cells from all germline lineages (ecto-, meso-, and endoderm), was obtained by pooling together undifferentiated mouse PSCs (E14TG2a obtained from ATCC, USA), whole mouse embryos (embryonic day 9.5 [E9.5] and E12.5), and maturing VM progenitors isolated from E10.5, E12.5, E14.5, and postnatal day 1 pups.

Human RNA, containing mixed cell populations, was generated by pooling undifferentiated human PSCs together with embryoid bodies (consisting of all germ layers), and varying maturation stages of VM neural progenitors and mature dopamine neurons (derived from differentiated human embryonic stem cells, as described below).

The H9 human embryonic stem cell line, expressing a green fluorescent reporter under the LMX1A promoter (H9 LMX1A-GFP), was cultured as previously described (Niclis et al., 2017b). Maintenance of pluripotency, prior to transplantation, was confirmed by morphology and the co-expression of OCT4 and SOX2 (Figures S1A–S1D). Undifferentiated hPSCs for transplantation were isolated by Accutase treatment and resuspended at 10,000 cells/μL.

To obtain a pool of purified neural progenitors of known origin, we differentiated PSCs to a VM fate as previously described (Niclis et al., 2017b), with correctly specified cells isolated by FACS for the GFP reporter gene, LMX1A. At 21 days *in vitro*, differentiating cultures were dissociated in Accutase to a single-cell suspension and FACS performed on a MoFlo cell sorter (Beckman Coulter). The generation of neural progenitors (of VM identity) was verified by co-expression of OTX2, FOXA2, and LMX1A (LMX1A-GFP[+]) (Figures S1E–S1I). As previously described, >95% of GFP^{+} cells co-expressed the ventral floorplate marker FOXA2 and forebrain-midbrain marker OTX2 (Niclis et al., 2017b), indicating that isolation of this GFP fraction (>80% of cells, Figure S1J) could enrich for correctly specified VM progenitors from the heterogeneous differentiated cultures by FACS. The FACS-isolated cell fraction was resuspended at 100,000 cells/μL in maturation medium and stored on ice until the time of implantation.

Cell Transplantation

All animal procedures were approved by The Florey Institute of Neuroscience and Mental Health Animal Ethics committee. Surgeries were performed on 30 athymic (Foxn1nu) nude mice under 2% isofluorane anesthesia. One microliter of cells was stereotaxically injected into the brains at the following coordinates, relative to bregma, as previously described (Kauhausen et al., 2013): 0.5 mm anterior, 2.1 mm lateral, and 3.2 mm below the surface of the dura. Transplant groups (n = 10/group) included: (1) undifferentiated hPSCs implanted for a period of 1 month; (2) VM progenitors, implanted for 1 month; and (3) VM progenitors, implanted for 6 months.

Tissue Processing and Histochemistry

After the prescribed period of graft survival (1 or 6 months), a subset of animals (n = 5/group) were killed by an overdose of sodium pentobarbitone (100 mg/kg), and transcardially perfused with 4% paraformaldehyde and cryosectioned. Immunohistochemistry was performed on fixed cell cultures or brain sections as previously described (Somaa et al., 2017). Primary antibodies and dilutions were as follows: 4′,6-diamidino-2-phenylindole (DAPI, 1 μg/mL; Sigma Aldrich), goat anti-FOXA2 (1:200; Santa Cruz Biotechnology), chicken anti-GFP (1:1,000; Abcam), rabbit anti-GFAP (1:800; DAKO), mouse anti-HNA (1:300; Millipore), rabbit anti-Ki67 (1:1,000; Thermo Fisher), mouse anti-NESTIN (1:200; Millipore), mouse anti-Neuroligin 3 (Nlgn3, 1:100; Synaptic Systems), mouse anti-OCT4 (1:100; Santa Cruz), rabbit anti-Olig1 (1:200; Millipore), rabbit anti-OTX2 (1:4,000; Millipore), mouse anti-PSA-NCAM (1:200; Santa Cruz), goat anti-SOX2 (1:200; R&D), mouse anti-synaptophysin (hSYP, 1:1,000; Enzo Life Sciences), sheep anti-TH (1:800; Pelfreeze), rabbit anti-TH (1:1,000; Pelfreeze). For quantification of HNA[+], Ki67^{+}, GFP[+], and TH^{+} cells, images were captured at 20× magnification using a Zeiss Axio Observer Z.1 epifluorescence microscope. The density of Nestin labeling (percentage of immunoreactive pixels) was assessed from captured images and analyzed using ImageJ software.

RNA Isolation and Real-Time qPCR

The remaining animals (n = 5/group) were killed, the brains removed, and the striatum (containing the transplant) dissected from surrounding tissues and snap frozen. Tissue was homogenized using a TissueLyser LT (Qiagen) and total RNA extracted using the RNeasy Mini Kit (Qiagen). RNA yield and integrity were assessed using a Nanodrop One spectrophotometer (ThermoFisher Scientific) and confirmed using a Qubit (Thermo Fisher Scientific) and Tapestation (Agilent). The RNA was analyzed by qPCR or RNA-seq (Figure 1A).

Species-specific primers were designed using Primer3 (Untergasser et al., 2012), aimed at containing a minimum of 5-bp mismatches between graft and host, or two mismatches in the 5 bp at the 3′ end between species. Primers were targeted manually to regions of dissimilarity (identified by blasting paralog genes) or using Primer-BLAST and selecting both the xenograft and host species (*Homo sapiens* and *Mus musculus*, respectively in the present context) under organism in the "Primer Pair Specificity Checking Parameters." This identified primers specific only to the xenograft species (i.e., human). All xenograft-specific primers used in this study are listed in Figure 1B. Lineage-specific genes were selected from established markers used in the characterization of embryoid bodies (Tsankov et al., 2015; D'Antonio et al., 2017), and genes associated with vascular/endothelial cell differentiation identified from the MGI Gene Ontology Browser and Park et al. (2013). Genes were selected for confirmation with xenograft-specific qPCR based on showing highly significant upregulation in undifferentiated/teratoma grafts compared with neural progenitor grafts.

First-strand reverse transcription of 500 ng of RNA into cDNA was conducted using the SuperScript VILO cDNA Synthesis Kit (Invitrogen) according to the manufacturer's recommendations. Real-time qPCR was carried out on 25 ng of cDNA using the SYBR GreenER qPCR SuperMix Universal (Invitrogen) and run on a Rotor-Gene 6000 (Qiagen). To control for the size of the xenograft, we identified a xenograft-specific reference (housekeeping) gene. PSMB4, MTHFD1, CHAMP2A, and HPRT1 were tested and PSMB4 selected as the optimal housekeeping gene due to its high specificity and stable expression across the three graft types (Figure S1K). All qPCR data were analyzed using the ΔΔCt method (Pfaffl, 2001), using the xenograft-specific reference gene and expressed relative to the undifferentiated grafts. Five independent biological replicates were analyzed per group.

RNA Sequencing

cDNA libraries (containing graft and host RNA) were prepared using the TruSeq stranded mRNA sample preparation kit (Illumina). For sequencing, the final cDNA concentration of each sample was adjusted to generate a target of 20 million xenograft-specific reads using the percentage xenograft RNA calculated from the qPCR data. Note that due to the low percentage of xenograft RNA in the Immature neuronal grafts, 5.5 million reads were targeted. Libraries were subjected to paired-end, 75-bp sequencing on an Illumina HiSeq 2000 platform (Illumina) with three independent biological replicates analyzed per group.

Analysis was conducted on the Galaxy web platform (Afgan et al., 2018) using the Galaxy Australia server, and using Bioconductor (Huber et al., 2015) in the statistical analysis environment R (https://www.R-project.org/). Alignment to the human genome (Hg38) was performed using HISAT2 (2.0.3.3). Paired concordant reads were then mapped against the mouse reference genome (mm10). Under our high-stringency approach, all reads that aligned to both the human and mouse genome were discarded, accounting for an average of 5% of human reads.

Read counts for each gene were generated using HTSeq-count (0.6.1) on union mode (Anders et al., 2015). Differential expression analysis and principal component analysis were conducted with DeSeq2 (2.11.38) (Love et al., 2014). Expression heatmaps and unsupervised clustering were performed on log-transformed row-scaled expression values using the gplots package in R (Pfaffl, 2001). Gene ontology enrichment analysis on biological process was performed using the DAVID gene ontology browser (Huang da et al., 2009). Lists of human transcription factors and axon guidance cues and receptors were sourced from the HumanTFDB (Hu et al., 2019) and the KEGG PATHWAY Database (Kanehisa et al., 2017) (hsa04360, *Homo sapiens* axon guidance), respectively. The RNA-seq data generated from this study has been deposited in NCBI's Gene Expression Omnibus and are accessible through series accession number GEO: GSE126804.

Statistical Analysis

All data are presented as mean ± SEM. Statistical tests employed (inclusive of one-way ANOVA and Student's t tests) are stated in the figure legends. Alpha levels of $p < 0.05$ were considered significant with all statistical analysis performed using GraphPad Prism: *$p < 0.05$, **$p < 0.01$, and ***$p < 0.001$.

REFERENCES

Afgan, E., Baker, D., Batut, B., van den Beek, M., Bouvier, D., Cech, M., Chilton, J., Clements, D., Coraor, N., Grüning, B.A., et al. (2018). The Galaxy platform for accessible, reproducible and collaborative biomedical analyses: 2018 update. Nucleic Acids Res. *46*, W537–W544.

Anders, S., Pyl, P.T., and Huber, W. (2015). HTSeq—a Python framework to work with high-throughput sequencing data. Bioinformatics *31*, 166–169.

Bariselli, S., Hornberg, H., Prevost-Solie, C., Musardo, S., Hatstatt-Burkle, L., Scheiffele, P., and Bellone, C. (2018). Role of VTA dopamine neurons and neuroligin 3 in sociability traits related to nonfamiliar conspecific interaction. Nat. Commun. *9*, 3173.

Barker, R.A., Parmar, M., Studer, L., and Takahashi, J. (2017). Human trials of stem cell-derived dopamine neurons for Parkinson's disease: dawn of a new era. Cell Stem Cell *21*, 569–573.

Bye, C.R., Jonsson, M.E., Bjorklund, A., Parish, C.L., and Thompson, L.H. (2015). Transcriptome analysis reveals transmembrane targets on transplantable midbrain dopamine progenitors. Proc. Natl. Acad. Sci. U S A *112*, E1946–E1955.

Cyranoski, D. (2018). 'Reprogrammed' stem cells implanted into patient with Parkinson's disease. Nat. News https://doi.org/10.1038/d41586-018-07407-9.

D'Antonio, M., Woodruff, G., Nathanson, J.L., D'Antonio-Chronowska, A., Arias, A., Matsui, H., Williams, R., Herrera, C., Reyna, S.M., Yeo, G.W., et al. (2017). High-throughput and cost-effective characterization of induced pluripotent stem cells. Stem Cell Reports 8, 1101–1111.

Doi, D., Samata, B., Katsukawa, M., Kikuchi, T., Morizane, A., Ono, Y., Sekiguchi, K., Nakagawa, M., Parmar, M., and Takahashi, J. (2014). Isolation of human induced pluripotent stem cell-derived dopaminergic progenitors by cell sorting for successful transplantation. Stem Cell Reports 2, 337–350.

Etzrodt, M., Endele, M., and Schroeder, T. (2014). Quantitative single-cell approaches to stem cell research. Cell Stem Cell 15, 546–558.

Hu, H., Miao, Y.R., Jia, L.H., Yu, Q.Y., Zhang, Q., and Guo, A.Y. (2019). AnimalTFDB 3.0: a comprehensive resource for annotation and prediction of animal transcription factors. Nucleic Acids Res. 47, D33–D38.

Huang da, W., Sherman, B.T., and Lempicki, R.A. (2009). Systematic and integrative analysis of large gene lists using DAVID bioinformatics resources. Nat. Protoc. 4, 44–57.

Huber, W., Carey, V.J., Gentleman, R., Anders, S., Carlson, M., Carvalho, B.S., Bravo, H.C., Davis, S., Gatto, L., Girke, T., et al. (2015). Orchestrating high-throughput genomic analysis with Bioconductor. Nat. Methods 12, 115–121.

Kanehisa, M., Furumichi, M., Tanabe, M., Sato, Y., and Morishima, K. (2017). KEGG: new perspectives on genomes, pathways, diseases and drugs. Nucleic Acids Res. 45, D353–D361.

Kantor, D.B., Chivatakarn, O., Peer, K.L., Oster, S.F., Inatani, M., Hansen, M.J., Flanagan, J.G., Yamaguchi, Y., Sretavan, D.W., Giger, R.J., et al. (2004). Semaphorin 5A is a bifunctional axon guidance cue regulated by heparan and chondroitin sulfate proteoglycans. Neuron 44, 961–975.

Kauhausen, J., Thompson, L.H., and Parish, C.L. (2013). Cell intrinsic and extrinsic factors contribute to enhance neural circuit reconstruction following transplantation in Parkinsonian mice. J. Physiol. 591, 77–91.

Kirkeby, A., Grealish, S., Wolf, D.A., Nelander, J., Wood, J., Lundblad, M., Lindvall, O., and Parmar, M. (2012). Generation of regionally specified neural progenitors and functional neurons from human embryonic stem cells under defined conditions. Cell Rep. 1, 703–714.

Kirkeby, A., Nolbrant, S., Tiklova, K., Heuer, A., Kee, N., Cardoso, T., Ottosson, D.R., Lelos, M.J., Rifes, P., Dunnett, S.B., et al. (2017). Predictive markers guide differentiation to improve graft outcome in clinical translation of hESC-based therapy for Parkinson's disease. Cell Stem Cell 20, 135–148.

Kriks, S., Shim, J.W., Piao, J., Ganat, Y.M., Wakeman, D.R., Xie, Z., Carrillo-Reid, L., Auyeung, G., Antonacci, C., Buch, A., et al. (2011). Dopamine neurons derived from human ES cells efficiently engraft in animal models of Parkinson's disease. Nature 480, 547–551.

La Manno, G., Gyllborg, D., Codeluppi, S., Nishimura, K., Salto, C., Zeisel, A., Borm, L.E., Stott, S.R.W., Toledo, E.M., Villaescusa, J.C., et al. (2016). Molecular diversity of midbrain development in mouse, human, and stem cells. Cell 167, 566–580.e19.

Love, M.I., Huber, W., and Anders, S. (2014). Moderated estimation of fold change and dispersion for RNA-seq data with DESeq2. Genome Biol. 15, 550.

Munoz-Sanjuan, I., and Brivanlou, A.H. (2002). Neural induction, the default model and embryonic stem cells. Nat. Rev. Neurosci. 3, 271–280.

Niclis, J.C., Gantner, C.W., Hunt, C.P.J., Kauhausen, J.A., Durnall, J.C., Haynes, J.M., Pouton, C.W., Parish, C.L., and Thompson, L.H. (2017a). A PITX3-EGFP reporter line reveals connectivity of dopamine and non-dopamine neuronal subtypes in grafts generated from human embryonic stem cells. Stem Cell Reports 9, 868–882.

Niclis, J.C., Gantner, C.W., Alsanie, W.F., McDougall, S.J., Bye, C.R., Elefanty, A.G., Stanley, E.G., Haynes, J.M., Pouton, C.W., Thompson, L.H., et al. (2017b). Efficiently specified ventral midbrain dopamine neurons from human pluripotent stem cells under xeno-free conditions restore motor deficits in parkinsonian rodents. Stem Cell Transl. Med. 6, 937–948.

Park, C., Kim, T.M., and Malik, A.B. (2013). Transcriptional regulation of endothelial cell and vascular development. Circ. Res. 112, 1380–1400.

Pfaffl, M.W. (2001). A new mathematical model for relative quantification in real-time RT-PCR. Nucleic Acids Res. 29, e45.

Samata, B., Doi, D., Nishimura, K., Kikuchi, T., Watanabe, A., Sakamoto, Y., Kakuta, J., Ono, Y., and Takahashi, J. (2016). Purification of functional human ES and iPSC-derived midbrain dopaminergic progenitors using LRTM1. Nat. Commun. 7, 13097.

Somaa, F.A., Wang, T.Y., Niclis, J.C., Bruggeman, K.F., Kauhausen, J.A., Guo, H., McDougall, S., Williams, R.J., Nisbet, D.R., Thompson, L.H., et al. (2017). Peptide-based scaffolds support human cortical progenitor graft integration to reduce atrophy and promote functional repair in a model of stroke. Cell Rep. 20, 1964–1977.

Tang, F., Barbacioru, C., Bao, S., Lee, C., Nordman, E., Wang, X., Lao, K., and Surani, M.A. (2010). Tracing the derivation of embryonic stem cells from the inner cell mass by single-cell RNA-Seq analysis. Cell Stem Cell 6, 468–478.

Trounson, A., and McDonald, C. (2015). Stem cell therapies in clinical trials: progress and challenges. Cell Stem Cell 17, 11–22.

Tsankov, A.M., Akopian, V., Pop, R., Chetty, S., Gifford, C.A., Daheron, L., Tsankova, N.M., and Meissner, A. (2015). A qPCR ScoreCard quantifies the differentiation potential of human pluripotent stem cells. Nat. Biotechnol. 33, 1182–1192.

Untergasser, A., Cutcutache, I., Koressaar, T., Ye, J., Faircloth, B.C., Remm, M., and Rozen, S.G. (2012). Primer3—new capabilities and interfaces. Nucleic Acids Res. 40, e115.

Wiese, C., Rolletschek, A., Kania, G., Blyszczuk, P., Tarasov, K.V., Tarasova, Y., Wersto, R.P., Boheler, K.R., and Wobus, A.M. (2004). Nestin expression—a property of multi-lineage progenitor cells? Cell. Mol. Life Sci. 61, 2510–2522.